Journal of Sound and Vibration (2000) **234**(2), 241–258
doi:10.1006/jsvi.1999.2876, available online at http://www.idealibrary.com on IDEAL®

ON THE TIME–FREQUENCY ANALYSIS OF SIGNALS THAT DECAY EXPONENTIALLY WITH TIME

S. K. TANG

Department of Building Services Engineering, The Hong Kong Polytechnic University, Hong Kong, People's Republic of China

(*Received* 15 *June* 1999, *and in final form* 19 *November* 1999)

The use of the short-time Fourier transform and the wavelet transform implemented using the new harmonic wavelets for analyzing the time variation of the spectral contents of exponentially time-decaying signals is studied in the present investigation. Focus is also placed on how well these methods can recover the decay constant of each frequency component in the signals in a relatively narrow bandwidth situation. Both artificial and experimentally recorded signals have been used. Results suggest that the short-time Fourier transform is in general more reliable than the wavelet transform for the present purpose. The short-time Fourier transform also gives excellent recovery of the decay constants if the signals are made up of discrete frequency components.

1. INTRODUCTION

Non-stationary signals appear in many branches of engineering. Examples include the vibration patterns of a diesel engine crank-shaft [1] and the turbulent pressure fluctuations within an air jet [2]. Both the frequency contents of these signals and their magnitudes vary with time so that the conventional Fourier transform method cannot deal with these signals properly. Rather, the approach of time–frequency analysis [3] provides a means to handle the problem.

The concept of time–frequency analysis is not a very new one. Owing to its importance in dealing with non-stationary signals, many algorithms for its implementation have been developed in the past few decades. Typical examples are the Wigner–Ville distribution [4], short-time Fourier transform [5] and more recently, the wavelet transform [6]. The advantages and drawbacks of these methods were discussed [7]. There are also studies showing that these methods are somewhat related to each other [8]. Newland [9, 10] suggests that the wavelets allow the changing spectral composition of a non-stationary signal to be measured and presented in the form of a time–frequency map and thus, are useful as a tool for vibration signal analysis. Nowadays, these is much research related to the engineering applications of wavelets. Some examples are the analysis of the responses of a slipping foundation by Basu and Gupta [11] and the investigation on flow turbulence by Farge [12].

Harmonic signals that decay exponentially with time appear frequently in the field of acoustics and vibration. The time constants of such decays describe the rate of energy loss and have significant applications. It is well known that the vibration signal of a slightly Coulomb damped vibrating system of one-degree-of-freedom decays exponentially with time and the time constant is important for the estimation of the damping ratio [13]. Also,

0022-460X/00/270241 + 18 $35.00/0

the decay of sound energy in a reverberant room with limited absorption shows an exponential relationship with time [13]. The time constant of such decay gives the reverberation time and thus an estimate of the sound absorption in the enclosure. Though there seems to be a general belief that the wavelets are very useful in the analysis of non-stationary signals and there are electronic devices that utilize them to measure the reverberation times of enclosures in octave bands [7], it appears to the author that the performance of the various time–frequency analysis methods on dealing with these important signals is not well understood. An example of this can be found in Martin *et al.* [14] where the time–frequency maps of a concert hall impulse response obtained by using four different approaches are very different so that it is very hard to conclude which one is correct.

In the present investigation, the short-time Fourier transform and the wavelet transform using the new harmonic wavelets developed by Newland [15] are performed on the exponentially time-decaying signals. These wavelets provide both variable and constant bandwidth transforms and thus are better than the conventional ones, such as the Gabor wavelets [16]. The focus here is on how these transforms reveal the time variations of the spectral contents and, more important, the decay constants of the signals. The present investigation deals with relatively narrow bandwidth situations. It is hoped that the results so obtained will provide useful information on the instrumentation selection for the studies of building acoustics and vibration.

2. THE TIME-FREQUENCY ANALYSIS METHODS

Only two transforms, the short-time Fourier transform (STFT) and the wavelet transform (WT), are studied in the present investigation as they are the most common ones used nowadays and are relatively easy to implement. In this section, the performance of these methods in handling an exponentially time-decaying signal is analyzed theoretically. The time signal $f(t)$ is assumed to take the form of

$$f(t) = A\mathrm{e}^{-\alpha t}\,\mathrm{e}^{\mathrm{j}\omega_0 t}, \tag{1}$$

where α is the decay constant, ω_0 the frequency of the signal and $A = f(0)$.

2.1. SHORT-TIME FOURIER TRANSFORM

A window function w is required in the STFT $F(\omega, \tau)$ as

$$F(\omega, \tau) = \frac{1}{2\pi}\int_{-\infty}^{\infty} f(t)\, w(t-\tau)\,\mathrm{e}^{-\mathrm{j}\omega t}\,\mathrm{d}t. \tag{2}$$

Substituting equation (1) into equation (2), F vanishes if $\omega \neq \omega_0$ and

$$F(\omega_0, \tau) = \frac{A}{2\pi}\int_{-\infty}^{\infty} \mathrm{e}^{-\alpha t}\, w(t-\tau)\,\mathrm{d}t = \frac{A}{2\pi}\,\mathrm{e}^{-\alpha\tau}\int_{-\infty}^{\infty} w(t')\,\mathrm{e}^{-\alpha t'}\,\mathrm{d}t'. \tag{3}$$

Since α is constant, it follows that the magnitude of $F(\omega_0, \tau)$ decays exponentially with the time position τ no matter what w is. Once α is found, A can be obtained. It should be noted

that the above discussion is valid for a signal having more than one harmonic component provided that the sampling rate and the frequency resolution are well chosen. However, it should be noted that STFT may not be able to deal with a very rapid rise of signal magnitude. One can deduce that when the unit step function $u(t - t_0)$ is added to the signal $f(t)$, equation (3) will become

$$F(\omega_0, \tau) = \frac{A}{2\pi} e^{-\alpha\tau} \int_{-\infty}^{\infty} u(t' + \tau - t_0)\, w(t')\, e^{-\alpha t'}\, dt' \tag{4}$$

so that $F(\omega_0, \tau)$ may not vanish for $\tau < t_0$. The magnitude of $F(\omega_0, \tau)$ decays exponentially with τ when $\tau - t_0$ is greater than half the window width. The major drawback of STFT is on its constant time and frequency resolutions. This is discussed in many papers (for instance, Newland [9]) and thus is not repeated here.

2.2. WAVELET TRANSFORM

The wavelet transform, $W(\tau)$, is defined as

$$W(\tau) = \int_{-\infty}^{\infty} f(t)\, g^*(t - \tau)\, dt, \tag{5}$$

where τ is the time position, g is the wavelet function and the asterisk denotes a complex conjugate [17]. The harmonic wavelets take the form

$$g(t) = \frac{\exp(j2n\pi t) - \exp(j2m\pi t)}{j2\pi t(n - m)}, \tag{6}$$

where m and n are real constants and $n > m$ [15]. The frequency resolution and the centre frequency of this transform are $2(n - m)\pi$ and $(n + m)\pi$ respectively. The major advantage of this type of wavelets over the traditional ones is that they provide high flexibility in the choice of transform bandwidth.

Substituting equations (1) and (6) into equation (5), one obtains

$$W(\omega, \tau) = Ae^{-\alpha t} e^{j\omega_0\tau} \int_{-\infty}^{\infty} \frac{e^{-\alpha t'} e^{j\omega_0 t'}}{j2\pi(n - m)t'} (e^{-j2\pi m t'} - e^{-j2\pi n t'})\, dt', \tag{7}$$

where $\omega = (n + m)\pi$. Though the magnitude of $W(\omega, \tau)$ decreases exponentially with time, the integral involved does not converge. In practice, there will be no signal for $t < 0$. If one considers

$$f(t) = Ae^{-\alpha t} e^{j\omega_0 t}\, u(t - t_0),$$

where u is the unit step function as in the case of STFT, then

$$W(\omega, \tau) = Ae^{-\alpha t} e^{j\omega_0\tau} \int_{t_0 - \tau}^{\infty} \frac{e^{-\alpha t'} e^{j\omega_0 t'}}{j2\pi(n - m)t'} (e^{-j2\pi m t'} - e^{-j2\pi n t'})\, dt',$$

and the integral exists. It can then be shown that

$$W(\omega, \tau) = \frac{e^{-\alpha\tau} e^{j\omega_0\tau}}{j2\pi(n-m)} (E_1(a(t_0-\tau)) - E_1(b(t_0-\tau))),$$

$$\Rightarrow |W(\omega, \tau)| = \frac{e^{-\alpha\tau}}{2\pi(n-m)} |E_1(a(t_0-\tau)) - E_1(b(t_0-\tau))| = \frac{e^{-\alpha\tau}}{2\pi(n-m)} \left| \int_{a(t_0-\tau)}^{b(t_0-\tau)} z^{-1} e^{-z} dz \right|, \tag{8}$$

where E_1 is the exponential integral [18], $a = \alpha + j(2\pi n - \omega_0)$ and $b = \alpha + j(2\pi m - \omega_0)$. Owing to the branch cut of e^{-z}/z, which is the negative real axis on the complex plane [19], $|W(\omega, \tau)|$ is relatively larger when $\tau > t_0$ and $2\pi m < \omega_0 < 2\pi n$. For $\omega_0 < 2\pi m$ or $\omega_0 > 2\pi n$, $|W(\omega, \tau)|$ is still finite. However, it can be shown at a fixed τ that the magnitude of the integral in equation (8) decreases with increasing difference between ω_0 and the centre frequency of the transform approximately as $(\alpha^2 + (\omega - \omega_0)^2)^{-0.5}$ for low-frequency resolution.

Therefore, the harmonic wavelets are in principle capable of distinguishing two time fluctuating components of relatively close frequencies upon a suitable choice of the bandwidth. This is essentially not true for the constant-Q-type wavelet transform. For example, if $g(t)$ is replaced by the Gabor wavelet

$$\frac{1}{\sqrt[4]{\pi}} \sqrt{\frac{\psi}{a\gamma}} \exp(-(\psi t/a\gamma)^2 + j\psi t/a)$$

where ψ, γ and a are constants,

$$|W(a, \tau)| = \frac{A\sqrt{\alpha\gamma}}{\sqrt[4]{\pi}} \exp(\gamma^2 a^2 \alpha^2/8\pi^2 - (2\pi - \omega_0 a)^2) e^{-\alpha\tau}. \tag{9}$$

Though the magnitude of this Gabor transform decays exponentially with τ, it can be observed that $|W|$ does not vanish very quickly within a relatively large neighbourhood about $a = 2\pi/\omega_0$. One can verify this by substituting $\omega_0 = \omega_1 + \Delta\omega$ $(\Delta\omega \to 0)$ and $a = 2\pi/\omega_1$ into equation (9).

3. MULTI-FREQUENCY SIGNALS

This section describes the performance of STFT and WT in the estimation of the decay constant of each frequency component in a signal. This signal may be artificial or obtained from the experiment. It can be noted that both methods are suitable for our purpose if the signal concerned contains only one frequency component and thus, this kind of signal will not be considered any further. In the present study, the Hann window [16] is used in the STFT.

3.1. SIGNAL WITH DISCRETE FREQUENCY COMPONENTS

We consider a signal containing three discrete frequency components:

$$f(t) = A_1 e^{-t/2} e^{j20\pi t} + A_2 e^{-t/4} e^{j30\pi t} + A_3 e^{-t} e^{j44\pi t}. \tag{10}$$

Figure 1(a) shows the time–frequency map of $20\log_{10}|F(\omega, \tau)|$ of $f(t)$ obtained using the STFT with 50% overlap and all As equal unity. The frequency resolution is 0·122 Hz. The

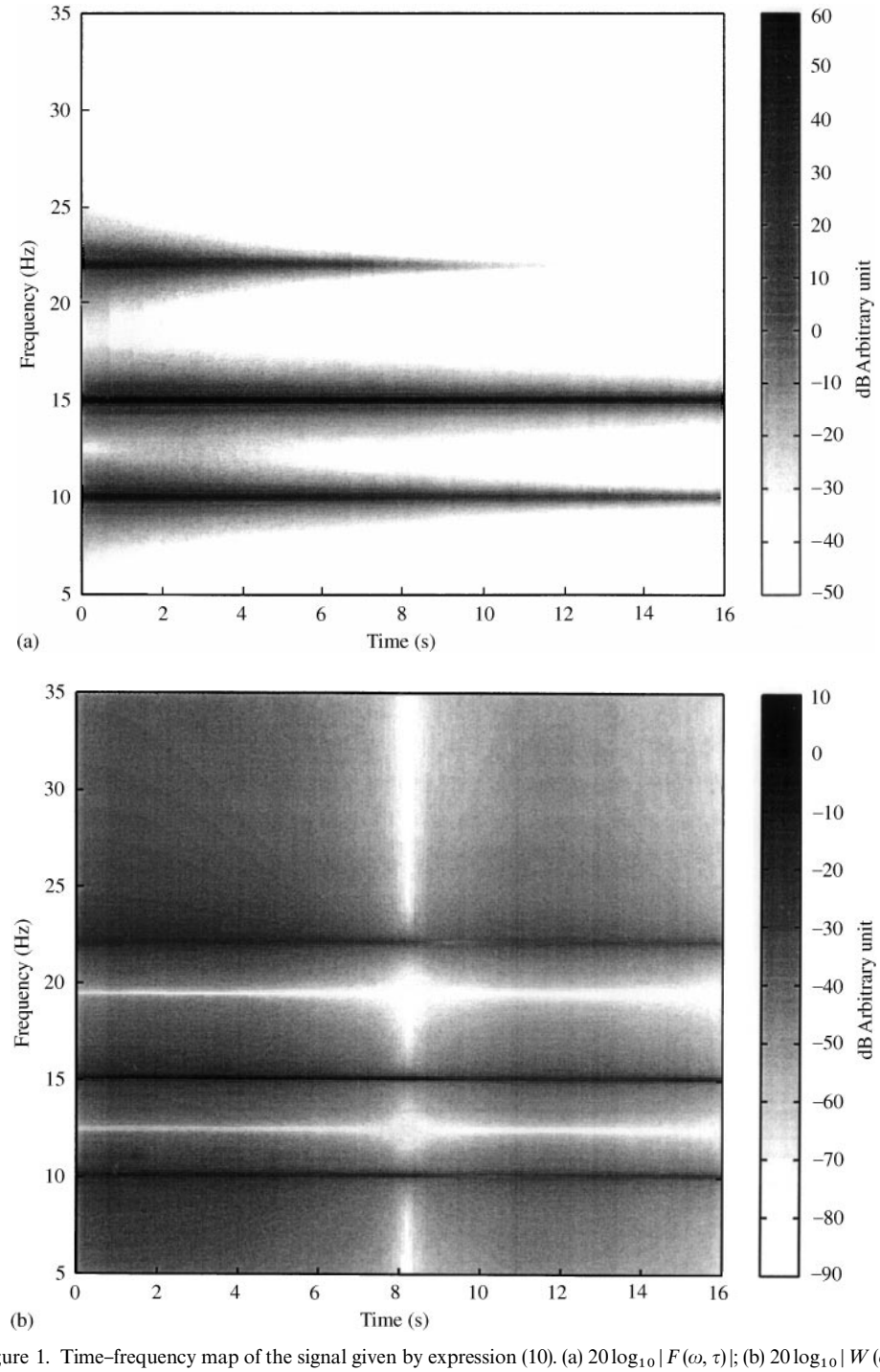

Figure 1. Time–frequency map of the signal given by expression (10). (a) $20\log_{10}|F(\omega,\tau)|$; (b) $20\log_{10}|W(\omega,\tau)|$.

distinctive frequency components are all recovered. However, the corresponding map of $20\log_{10}|W(\omega,\tau)|$ obtained from WT by using the FFT method of Newland [17] looks disappointing (Figure 1(b)), though the major frequency components are recovered. The situation is greatly improved when the bandwidth is increased to about 5 Hz or if the

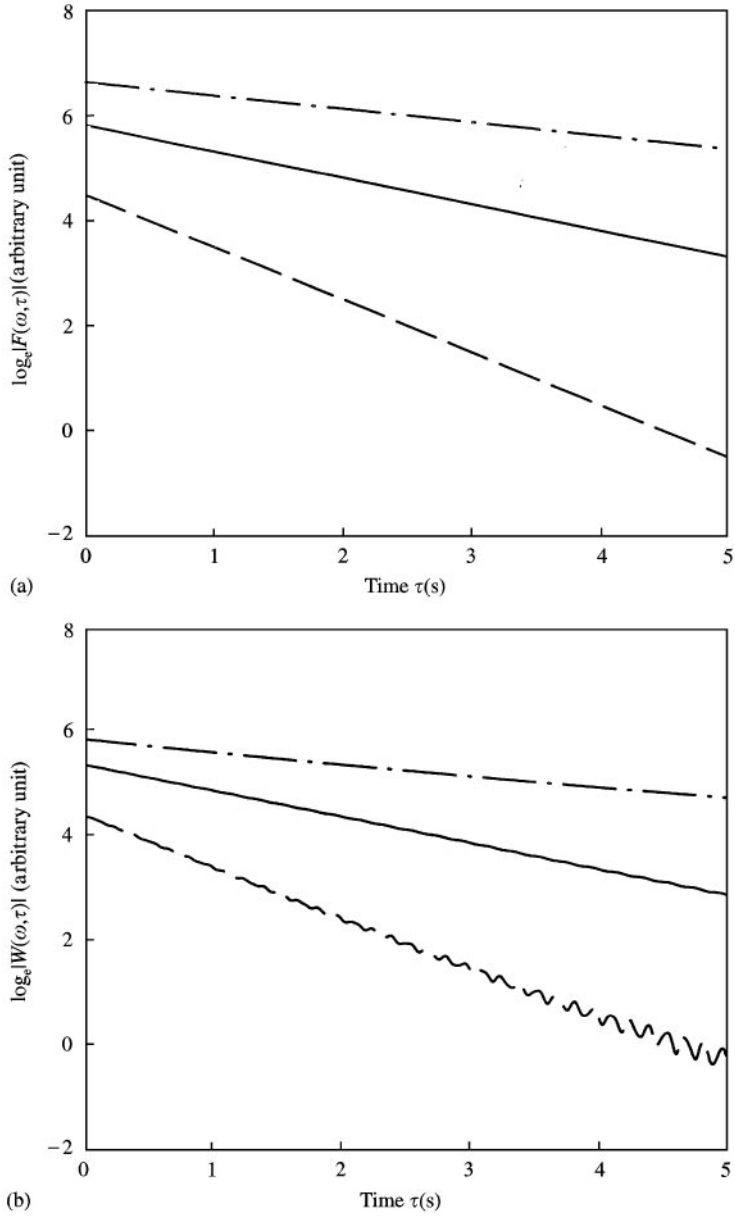

Figure 2. Time–decay curves of frequency components in expression (10). (a) STFT; (b) WT: ——, 10 Hz; – · –, 15 Hz; — —, 22 Hz.

convolution formula (equation (5)) is employed. The corresponding map of $20\log_{10}|W(\omega,\tau)|$ is very similar to Figure 1(a) and thus is not presented. In the foregoing discussions, all maps related to WT, unless otherwise stated, are obtained by using equation (5).

Figures 2(a) and 2(b) show the time decays of the three components in $f(t)$ recovered using STFT and WT respectively. The decay constants obtained from STFT are excellent and they do not depend on the percentage of overlapping. Some irregularities are observed

on the time decay curves obtained by WT (Figure 2(b)). While the decay constants of the 10 and 22 Hz components are retrieved by WT with high accuracy, that of the 15 Hz component is 0·22, which is about 10% lower than the right value (0·25). The results obtained using the constant-Q-type wavelet transform are poor and thus are not included in the present paper.

3.2. EXPONENTIALLY DECAYING BROADBAND SIGNALS

The first type of signal considered in this section is a white noise $n(t)$ with a decay factor $e^{-t/4}$ (Figure 3). Thus, $f(t) = n(t)e^{-t/4}$. The white noise is produced numerically by the algorithm of Kuo and Morgan [20]. We analyze the time decay of each narrow frequency band to see whether the correct decay constant can be found. In general, the broadband signals will result in very rough time decaying curves and thus, the backward integration method of Schroeder [21] is applied to determine the decay constants in this section.

Figure 4 illustrates the variation of decay constants with frequency obtained by STFT and WT. The frequency resolution Δf is 0·98 Hz. For STFT, a 50% overlap is adopted. Though STFT does not reveal the exact decay constant for each frequency component, the mean is at 0·25 s^{-1} and the standard deviation (S.D.) is 0·019 s^{-1}. This tends to show that the results of STFT are still satisfactory. The corresponding results obtained from WT fluctuate across the whole frequency range with a mean of 0·27 s^{-1} and an S.D. of 0·045 s^{-1}. It can be shown by the statistical inferential method [22] that the results obtained from WT differ considerably from 0·25 at the 95% confidence level. These two data sets also differ from each other at the 95% confidence level. WT does not perform with reasonable accuracy for this decaying white noise.

The second signal considered in this section is a broadband one with frequency components of different decay rates so that the magnitudes of the frequency components are

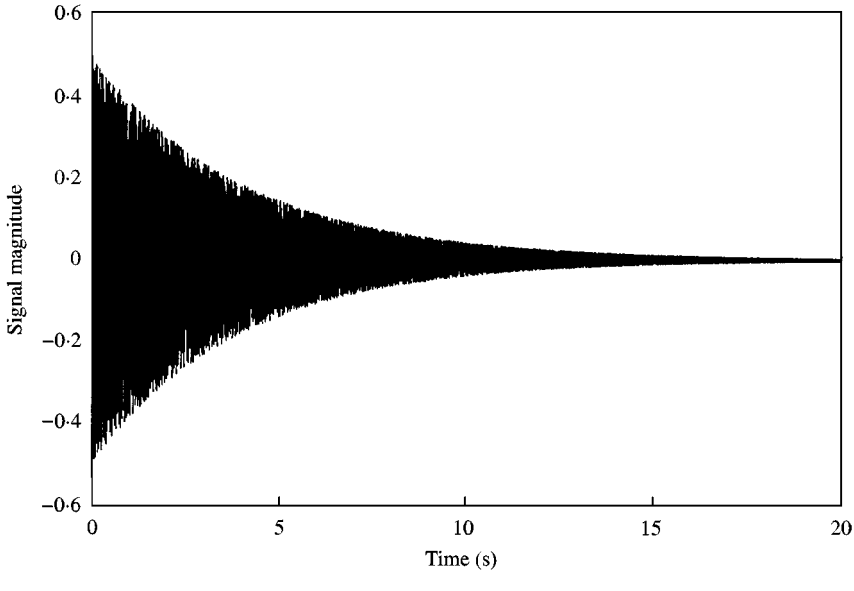

Figure 3. A white noise decaying exponentially with time.

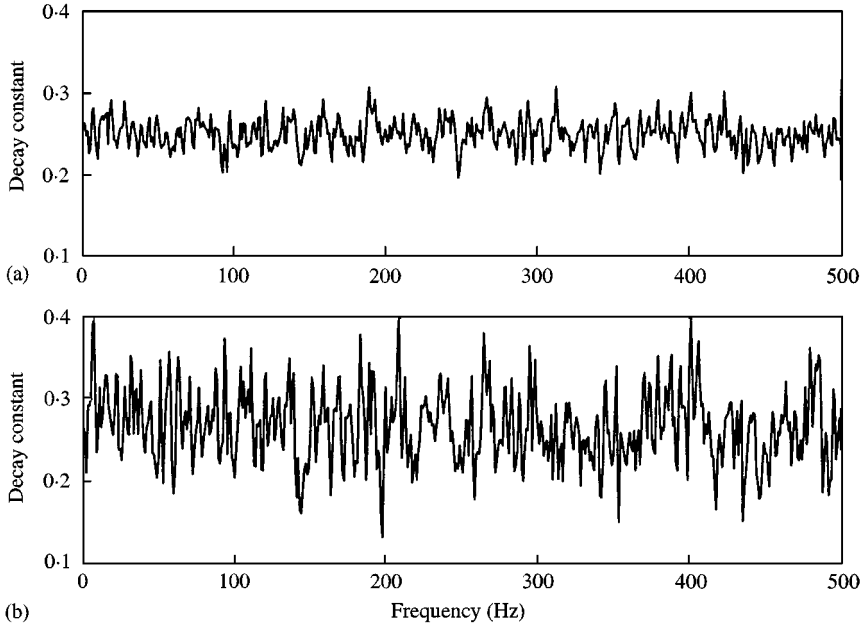

Figure 4. Variation of decay constants of white noise (Figure 3) with frequency. (a) STFT; (b) WT.

different for $t > 0$:

$$f(t) = \sum_{i=1}^{N} e^{-\alpha_i t} e^{-j(\omega_i t + \phi_i)}, \tag{11}$$

where α_i and $\omega_i/2\pi(=f_i)$ are the decay constant and frequency of the ith component, respectively, and ϕ_i a random phase factor. Without loss of generality, the sampling rate f_s is assumed to be 1000 Hz and $N = 512$. Also, $\omega_{i+1} - \omega_i = \pi f_s/N = \omega_1$. This kind of signal is important in room acoustics where the sound absorption of an enclosed space increases with frequency [13].

The signal considered is shown in Figure 5. It is the real part of equation (11) with $\alpha_i = 0{\cdot}8 - 0{\cdot}5\,((i - 512)/512)^2$. This choice of α_i, though arbitrary, can still reflect the reality in room acoustics where the sound absorption coefficient increases with sound frequency. It can be observed that the sum of the frequency components produces a time fluctuation that does not appear to decay exponentially with time. This kind of decay curve is commonly found in the measurement of room impulse response.

The dashed lines in Figure 6 show the contours of the time–frequency map of the signal in Figure 5 obtained using STFT with 50% overlap. The solid lines represent the exact results obtained directly from equation (11). The matching is very good, suggesting that STFT reveals correctly the decay constants α_is as well as the time variations of the spectral details of the signal. Figure 7 summarizes the variation of the decay constant with frequency obtained by WT. The performance of WT is satisfactory over the whole frequency range except near the low and high ends of the range. The corresponding results obtained by STFT collapse well with the theoretical curve and thus are not included in Figure 7.

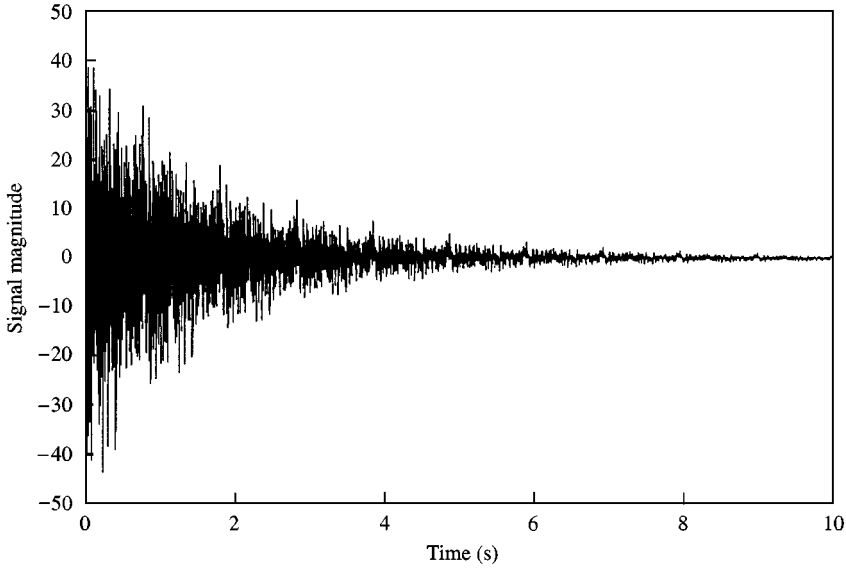

Figure 5. Broadband signal with decay rate that varies with frequency.

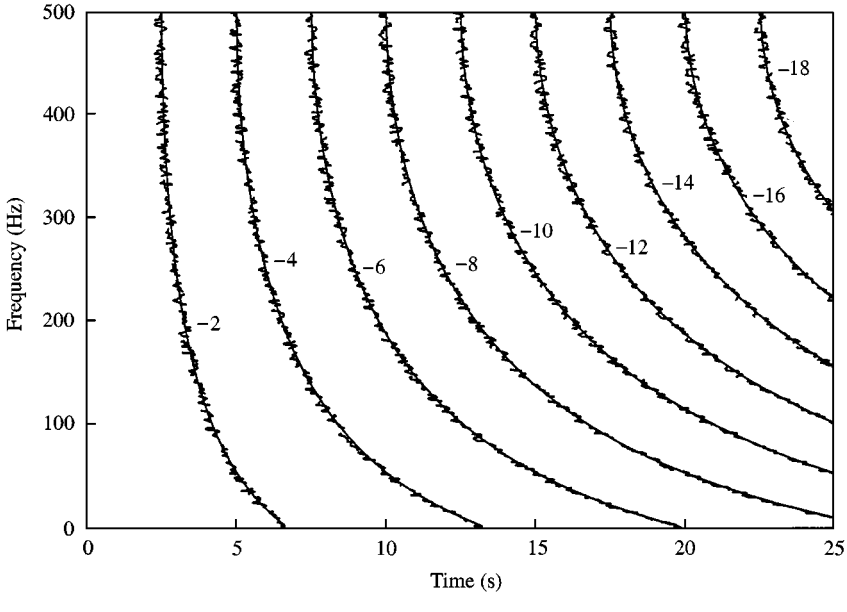

Figure 6. Time–frequency distribution of spectral energy of broadband signal (Figure 5). ——, Ideal; — — , STFT.

3.3. EXPERIMENTAL VIBRATION SIGNAL

The signal in this section was obtained experimentally from an accelerometer mounted firmly to the edge of a wooden board supported on four springs and there was a mass symmetrically clamped on the board. The wooden board was set into vibration by releasing

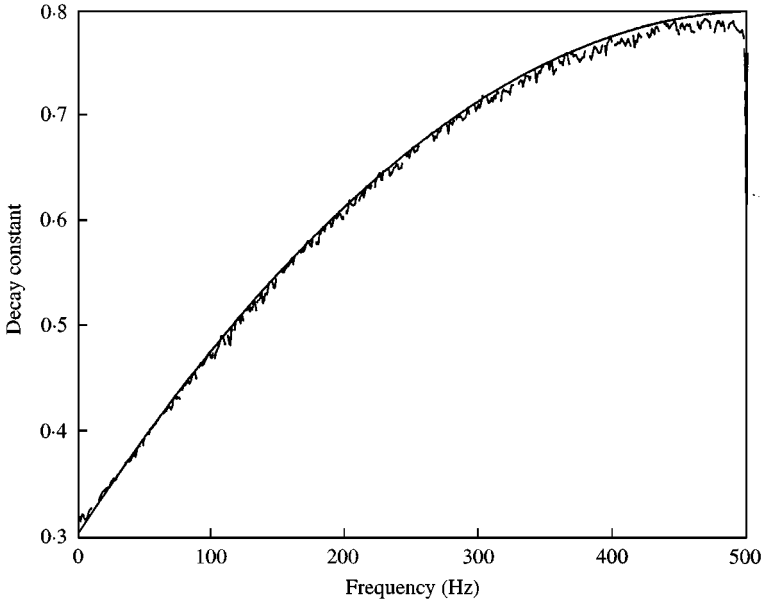

Figure 7. Variation of decay constant with frequency obtained by the wavelet transform. ——, $\alpha_i = 0{\cdot}8–0{\cdot}5((i - 512)/512)^2$; – – –, WT.

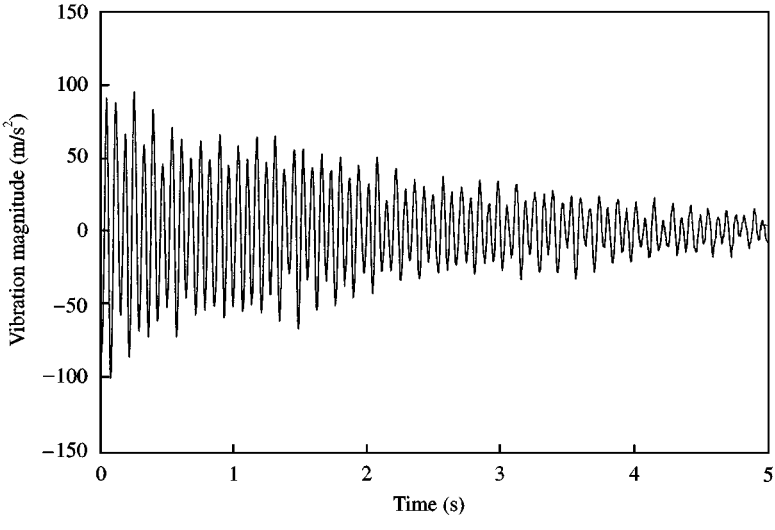

Figure 8. Vibration signal from accelerometer.

a force initially applied vertically onto the mass. No artificial damping material was involved and thus air was the main source of damping. One can expect that there will be six modes of vibration due to the six degrees of motion freedom. Also, the mode frequencies are not expected to be high.

The vibration signal is shown in Figure 8, which resembles the artificial signal of equation (10). It is obvious that this signal contains several low-frequency components overlapping

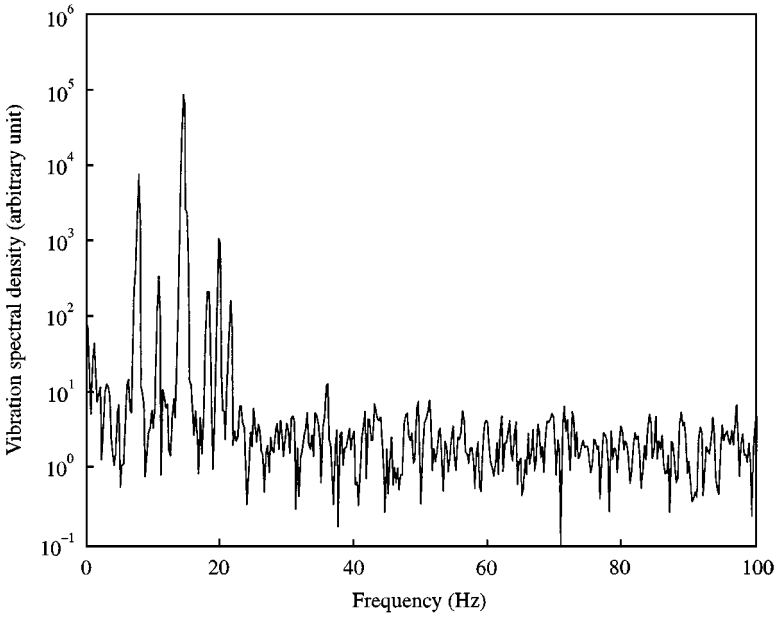

Figure 9. Spectrum of vibration signal (Figure 8) obtained by conventional Fourier transform.

with each other. Figure 9 gives the results obtained from the conventional Fourier transform taken over the whole period of measurement with a frequency resolution of about 0·23 Hz. It can be observed that there are prominent spectral peaks at 7·7, 10·8, 14·3, 18·0, 19·7 and 21·6 Hz, which should be related to the six modes of vibration. The vibration signal thus contains six discrete frequency components as expected.

The time–frequency maps obtained from STFT and WT with a frequency resolution of 0·23 Hz are presented in Figures 10(a) and 10(b) respectively. The STFT reveals clearly the existence of the six vibration modes. However, the WT gives a noisier map and can only reveal the three relatively stronger frequency components. Other components are not clearly recovered. The situation is worse at lower frequencies. Also, the frequency peaks in the WT time-frequency map are not as distinctive as those obtained by STFT at τ near to 0 (Figure 11).

Figure 12 shows the time variations of the magnitudes of the three major components in the vibration signal recovered by STFT and WT (7·7, 14·3 and 19·7 Hz). It is noticed that the results at 14·3 Hz obtained from STFT reveal an approximately exponential time decay at τ approximately greater than 1 s. For the other two components, the signature of exponential decay starts from $\tau = 0$ s. The corresponding data from WT do not indicate any possibility of having exponential decay signal. This situation is not improved even after applying the backward integration. Since the vibration velocity of the wooden board is small, the air damping force is in general proportional to velocity of motion. This should lead to an exponential time decay of the magnitude of each frequency component in the vibration signal. The results from STFT appear more reasonable and logical.

3.4. IMPULSE RESPONSE OF A ROOM

The final signal considered in the present investigation was obtained from a sound pulse created inside a reverberant room. It is expected that the low-frequency components can

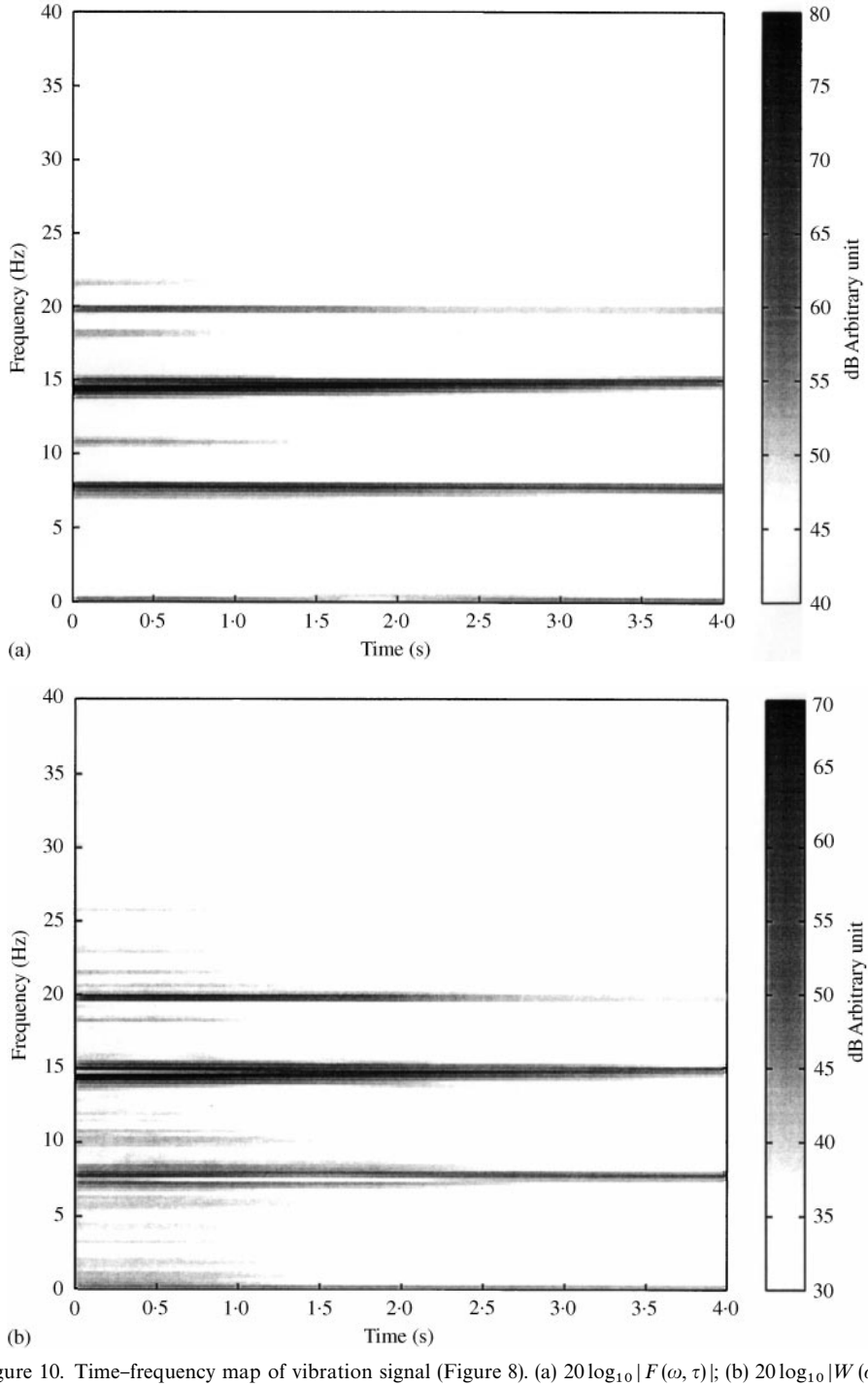

Figure 10. Time–frequency map of vibration signal (Figure 8). (a) $20\log_{10}|F(\omega,\tau)|$; (b) $20\log_{10}|W(\omega,\tau)|$.

undergo several reflections at the room boundaries while the high-frequency ones decay relatively quickly with time. The signal being analyzed, which is also the impulse response of the room, is shown in Figure 13. It is typical in room acoustics. It also looks similar to the broadband signal shown in Figure 6. The sampling rate was 12 000 samples/s and the

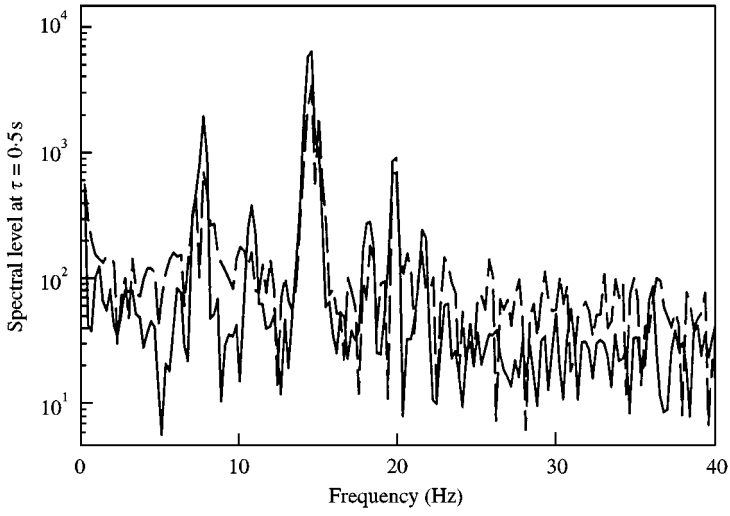

Figure 11. Spectral contents of vibration signal at $\tau = 0{\cdot}5$ s: ——, STFT; – –, WT.

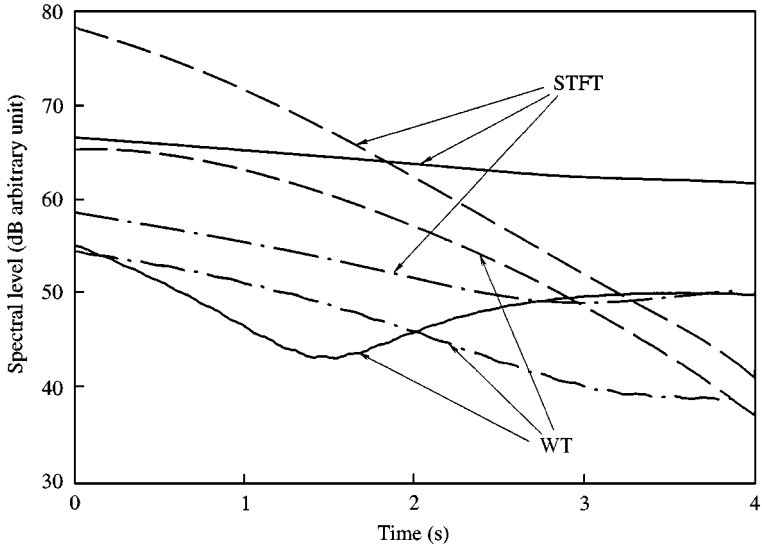

Figure 12. Time variations of frequency component magnitudes: ——, 7·7 Hz; – –, 14·3 Hz; – · –, 19·7 Hz.

anti-aliasing filter was applied to provide a low pass at 5000 Hz. Since we are dealing with room reverberation in this section, the frequency resolution need not be high as in many studies of room acoustics (for instance, Hodgson *et al.* [23]).

Figure 14(a) shows the time–frequency map of the room impulse response obtained by STFT with a frequency resolution of about 23·5 Hz and 50% overlap without backward integration. The pulse contains higher energy within the frequency band from about 100 to 1100 Hz. The low spectral values of frequencies below 100 Hz may be due to the sound source or the acoustical property of the room, which are outside the scope of the present study. The map also suggests that there is a 2100 Hz sound prevailing throughout the

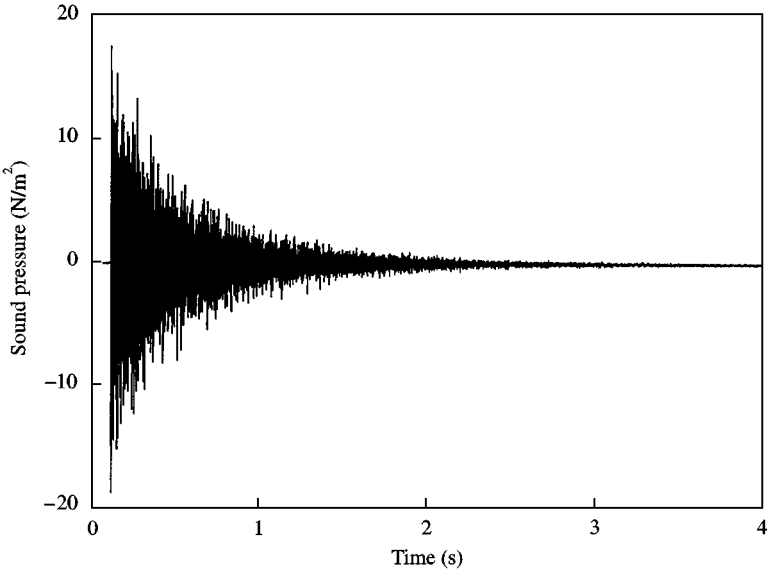

Figure 13. Impulse response of sample room.

measurement. This frequency component also exists in the signal before the pulse and is thus believed to be a noise from some building services equipment. It should be noted that STFT was not able to recover clearly the instant when the pulse reached the microphone. The decays of all the spectral levels are substantially linear with time (not shown here). No evidence of strong echo has been found.

The corresponding time–frequency map obtained by WT using the FFT method of Newland [17] without backward integration is shown in Figure 14(b). The frequency resolution of this calculation is 23·5 Hz. Figure 14(b) also reveals the higher energy content at frequencies below 1100 Hz and the weak energy content at frequencies below 100 Hz. However, the instant the pulse reached the microphone is not very clearly recovered. Basically, Figure 14(b), though with many noises especially at increased time, looks similar to Figure 14(a). This appears very different from those of Martin *et al.* [14] where STFT and WT (constant-Q type) gave different results in the analysis of the impulse response of a hall. One can also notice from Figure 14(b) that the prevailing 2100 Hz noise is not revealed by WT, suggesting that STFT may perform better in this analysis. Besides, the results presented in Figures 10 and 14 tend to suggest that the STFT can provide a better signal-to-noise ratio.

The reverberation times shown in Figure 15 are calculated from the decay constants determined from Figure 14 after applying the backward integration. The corresponding data obtained by direct one-third octave band filtering are also include in Figure 15 as a reference. Direct constant narrow-bandwidth filtering of the signal to determine the decay rates was not attempted because the associated zero phase-shift digital filters may not be reliable as the desired frequency resolution in the present time–frequency analysis is only around 0·2% of the sampling rate. The conventional Sabine's or Eyring's formulae [13] for the reverberation time calculation are not used here as the sound absorption coefficients of the room boundaries are not exactly known. Since the components having frequencies below 100 Hz are weak (Figure 14), the discussion is focussed on the frequency range between 100 and 5000 Hz.

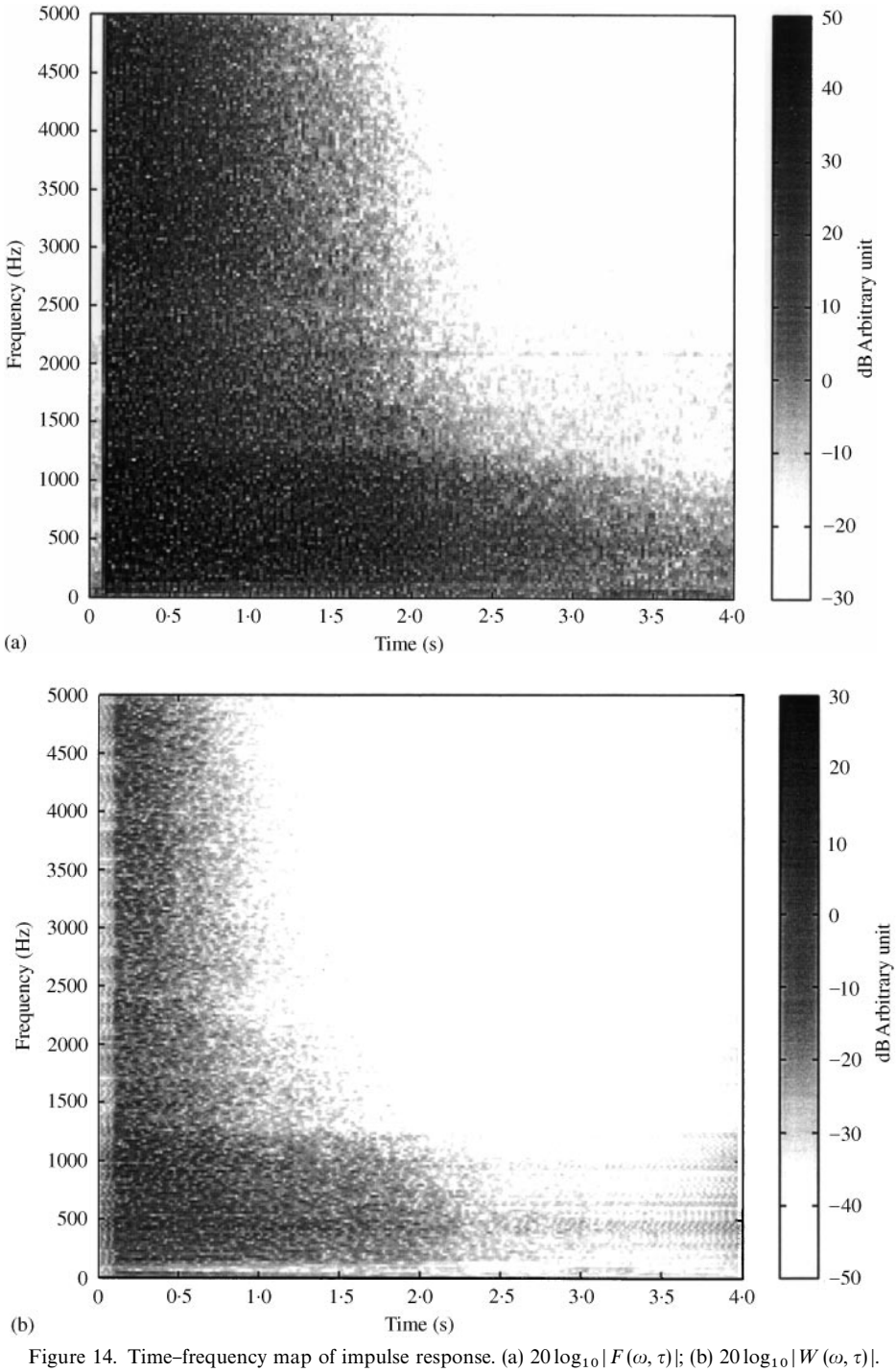

Figure 14. Time–frequency map of impulse response. (a) $20\log_{10}|F(\omega,\tau)|$; (b) $20\log_{10}|W(\omega,\tau)|$.

As expected, low-frequency noise appears to have a longer decay time than the higher frequency ones. It can also be observed from Figure 15(a) that the reverberation times obtained from STFT agree in principle with those obtained by the direct digital filtering method in the whole frequency range, especially at frequencies below 1000 Hz. These

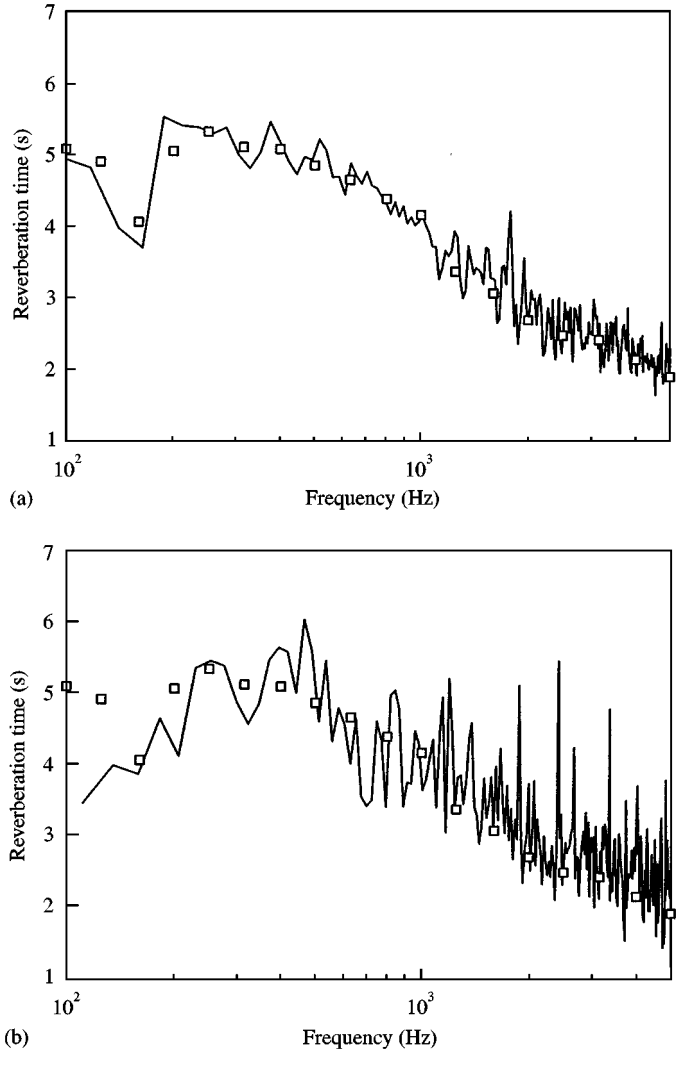

Figure 15. Variation of reverberation time with frequency. (a) STFT; (b) WT: ——, computed from transforms; □, one-third octave bands.

frequency components contain the majority of the sound energy. The results of WT scatter seriously at frequencies above 1000 Hz. This is due to the non-linear decay curves obtained after the backward integration at some frequencies (not shown here). This higher degree of scattering is consistent with the results of the white-noise decay shown in Figure 4. The results of WT at low frequencies are again not satisfactory.

4. CONCLUSIONS

In the present investigation, the performance of the short-time Fourier transform and the wavelet transform using the new harmonic wavelets on resolving the decay constants of exponentially time-decaying signals is studied. Both artificial and experimental signals are

used. A brief theoretical analysis on the issue is also given. This paper is focused on narrow and constant bandwidth applications.

Results show that both time-frequency methods work satisfactorily if the time-decaying signal contains only one frequency component. However, when multi-frequency or broadband signals are concerned, whether they are artificially generated or obtained from experiments, the short-time Fourier transform can recover the dominant frequency components and the corresponding decay constants with a reliable accuracy. The associated results do not depend on the percentage of overlap.

The wavelet transform implemented by the harmonic wavelets produces accurate results for artificial discrete signals. Though with larger scattering, it recovers the decay constants of broadband signals within engineering acceptable accuracy. However, this transform does not perform satisfactorily on the vibration signal and room impulse response obtained from experiments. It can only recover the relatively stronger frequency components from the vibration signal and gives rise to significant error when resolving the reverberation times of relatively higher-frequency components in a room impulse response. Its performance at low frequencies is also not satisfactory.

The present results suggest that the short-time Fourier transform performs better than the variable bandwidth wavelet transform in analyzing exponentially decaying signals, especially those obtained from experiments.

ACKNOWLEDGMENT

The assistance of Wilson Woo and Clement Lo in measuring the vibration and room impulse response signals is gratefully appreciated.

REFERENCES

1. R. B. RANDALL 1987 *Frequency Analysis*. Nærum, Denmark: Brüel & Kjær.
2. S. K. TANG and N. W. M. KO 1994 *Experiments in Fluids* **17**, 147–157. Coherent structure interactions in an unexcited coaxial jet.
3. P. FLANDRIN 1988 *IEEE Transactions on Acoustics, Speech, and Signal Processing* **36**, 1377–1384. A time-frequency formulation of optimum detection.
4. T. J. WAHL and J. S. BOLTON 1993 *Journal of Sound and Vibration* **163**, 101–122. The application of the Wigner distribution to the identification of structure-borne noise components.
5. C. H. HODGES, J. POWER and J. WOODHOUSE 1985 *Journal of Sound and Vibration* **101**, 203–218. The use of the sonogram in structural acoustics and an application to the vibrations of cylindrical shells
6. I. DAUBECHIES 1990 *IEEE Transactions on Information Theory* **36**, 961–1005. The wavelet transform, time–frequency localization and signal analysis.
7. S. GADE and K. GRAM-HANSEN 1996 *Brüel & Kjær Technical Reviews No*. 2. Non-stationary signal analysis using wavelet transform, short-time Fourier transform and Wigner–Ville distribution.
8. M. R. DELLOMO and G. M. JACYNA 1991 *Journal of the Acoustical Society of America* **89**, 2355–2361. Wigner transforms, Gabor coefficients, and Weyl-Heisenberg wavelets.
9. D. E. NEWLAND 1994 *Transactions of the American Society of Mechanical Engineers, Journal of Vibration and Acoustics* **116**, 409–416. Wavelet analysis of vibration, Part I: theory.
10. D. E. NEWLAND 1994 *Transactions of the American Society of Mechanical Engineers, Journal of Vibration and Acoustics* **116**, 417–425. Wavelet analysis of vibration, Part 2: wavelet maps.
11. B. BASU and V. K. GUPTA 1999 *Journal of Sound and Vibration* **222**, 547–563. Wavelet-based analysis of the non-stationary response of a slipping foundation.
12. M. FARGE 1992 *Annual Review of Fluid Mechanics* **24**, 395–457. Wavelet transforms and their applications to turbulence.

13. D. D. REYNOLDS 1981 *Engineering Principles of Acoustics: Noise and Vibration Control*. Boston: Allyn and Bacon.
14. N. MARTIN, J. MARS, J. MARTIN and C. CHORIER 1995 *IEEE Transactions on Signal Processing* **43**, 1842–1854. A Capon's time-octave representation application in room acoustics.
15. D. E. NEWLAND 1994 *Proceedings of the Royal Society of London. Series A* **444**, 605–620. Harmonic and musical wavelets.
16. A. D. POULARIKAS 1999 *The Handbook of Formulas and Tables for Signal Processing*. Boca Raton, FL: CRC Press.
17. D. E. NEWLAND 1999 *Transaction of the American Society of Mechanical Engineers: Journal of Vibration and Acoustics* **121**, 149–155. Ridge and phase identification in the frequency analysis of transient signals by harmonic wavelets.
18. I. S. GRADSHTEYN and I. M. RYZHIK 1965 *Table of Integrals, Series and Products*. New York: Academic Press.
19. F. W. J. OLVER 1974 *Asymptotics and Special Functions*. New York: Academic Press.
20. S. M. KUO and D. R. MORGAN 1996 *Active Noise Control Systems: Algorithms and DSP Implementations*. New York: Wiley.
21. M. R. SCHROEDER 1965 *Journal of the Acoustical Society of America* **37**, 409–412. New method of measuring reverberation time.
22. D. SCHIFF and R. B. D'AGOSTINO 1996 *Practical Engineering Statistics*. New York: Wiley.
23. M. HODGSON, R. REMPEI and S. KENNEDY 1999 *Journal of the Acoustical Society of America* **105**, 226–233. Measurement and prediction of typical speech and background noise levels in university classrooms during lectures.